Region-Selective Self-Assembly of Functionalized Carbon Allotropes from Solution

Zhenxing Wang,[†] Saeideh Mohammadzadeh,[†] Thomas Schmaltz,[†] Johannes Kirschner,[†] Artoem Khassanov,[†] Siegfried Eigler,[‡,§] Udo Mundloch,[‡,§] Claudia Backes,[‡,§,⊥] Hans-Georg Steinrück,[∥] Andreas Magerl,[∥] Frank Hauke,[‡,§] Andreas Hirsch,[‡,§] and Marcus Halik[†,*]

[†]Organic Materials & Devices (OMD), Institute of Polymer Materials, University Erlangen-Nürnberg, Martensstraße 7, 91058 Erlangen, Germany, [‡]Department of Chemistry and Pharmacy, University Erlangen-Nürnberg, Henkestraße 42, 91054 Erlangen, Germany, [§]Institute of Advanced Materials and Processes (ZMP), University Erlangen-Nürnberg, Dr.-Mack-Straße 81, 90762 Fürth, Germany, [⊥]School of Physics and CRANN, Trinity College Dublin, Dublin 2, Ireland, and [∥]Crystallography and Structural Physics, University Erlangen-Nürnberg, Staudtstraße 3, 91058 Erlangen, Germany

ABSTRACT Approaches for the selective self-assembly of functionalized carbon allotropes from solution are developed and validated for 0D-fullerenes, 1D-carbon nanotubes and 2D-graphene. By choosing the right molecular interaction of self-assembled monolayers (serving the surface) with the functionalization features of carbon materials, which provide the solubility but also serve the driving force for assembly, we demonstrate a region-selective and self-terminating assembly of the materials. Active layers of the carbon allotropes can be selectively deposited in the channel region of thin-film transistor (TFT) devices by this approach. As an example for a 0D system, molecules of C_{60} functionalized octadecylphosphonic acids are used to realize self-assembled monolayer field-effect transistors (SAMFETs) based on a selective molecular exchange reaction of stearic acid in the channel region. For noncovalently functionalized single-walled carbon nanotubes (SWCNTs) and graphene oxide (GO) flakes, the electrostatic Coulomb interactions between the functional groups of the carbon allotropes and the charged head groups of a SAM dielectric layer are utilized to implement the selective deposition.

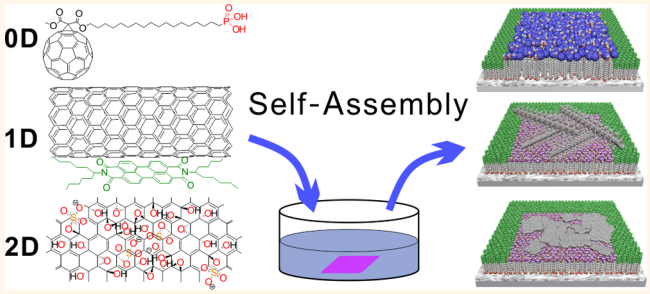

KEYWORDS: carbon allotropes · self-assembly · dip-coating · self-assembled monolayer · fullerene · carbon nanotubes · reduced graphene oxide

In the last decades, discoveries of new sp^2-carbon allotropes, such as fullerenes, carbon nanotubes and graphene, have significantly accelerated the interest in modern electronics beyond silicon.[1−6] Thereby, the extraordinary properties which vary with the dedicated dimensionality of the carbon allotropes enable almost all required electrical features to create carbon-based electronics and optoelectronics even on flexible substrates and/or large areas.[7−11] Fullerenes, representing the family of 0D carbon allotropes, exhibit strong acceptor properties and perform as n-type semiconductor or charge storage unit.[11,12] Single-walled carbon nanotubes (SWCNTs), by owning a very high aspect ratio, stand for the 1D system. Their metallic characteristics as well as semiconducting features with band gaps up to 2.0 eV, depending on the chirality, enable a variety of applications.[13,14] The semimetal graphene, as a 2D example, shows a huge charge carrier mobility, especially beneficial for analogue electronic applications, in which a pronounced band gap is actually not essential.[5,6,15] Although the high performance electronics based on carbon allotropes realized outstanding achievements, the material synthesis, as well as the fabrication processes, is still quite expensive and considerably complicated, and the compatibility with large-scale production remains challenging.[11,16−18] Solution processing of carbon allotropes, on the other hand, offers the prospect to overcome those difficulties.

Although the sp^2-conjugation in the allotropes is essential for the electrical transport properties, it limits the access to individually

* Address correspondence to marcus.halik@ww.uni-erlangen.de.

Received for review October 21, 2013 and accepted November 25, 2013.

Published online November 25, 2013
10.1021/nn405488n

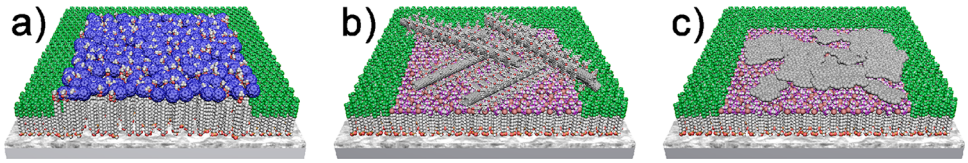

Figure 1. Schematic illustration of the region-selective deposition of carbon allotropes. (a) $C_{60}C_{18}$−PA (with blue C_{60} head groups) by exchange reaction as 0D example. (b) Network of noncovalently functionalized SWCNTs as 1D example and (c) GO flakes as 2D example. The outside regions with green head groups represent $F_{15}C_{18}$−PA SAM. The inside regions of (b) and (c) with purple head groups represent IMI-C_{12}−PA SAM.

dispersed species, due to the strong $\pi-\pi$ stacking. To overcome the interlayer or intermolecular $\pi-\pi$ stacking force, several concepts have been investigated to solubilize or disperse carbon allotropes. Typically, those concepts can be classified into the covalent approaches with functional groups attached to some carbon atoms or noncovalent approaches based on the electrostatic interactions with ligands. The most prominent example for direct covalent functionalization is the conversion of the almost insoluble C_{60} fullerene to the phenyl-C_{61}-butyric acid methyl ester (PCBM),[19] which introduces solubility but in general preserves the electronic structure of C_{60}, due to the controlled exohedral attachment of only one functional group.[12,20] To generate well-dispersed SWCNTs, both approaches including noncovalent wrapping with polymers or π-ligands as well as covalent motives have been successfully exploited.[21−24] Another example, which illustrates the challenges in covalent functionalization, is the oxidation of graphene (starting from graphite) to graphene oxide (GO). This leads to a highly disturbed π-system and consequently degraded electrical properties of the GO, so that an additional reductive back conversion to reduced graphene oxide (rGO) is required after processing to achieve graphene-like properties.[25−27]

However, a sufficient dispersion of the active carbon materials is just the initial step to realize solution-processed electronic devices. Even more important is the controlled and preferred self-aligned integration of the materials into device architectures from solution. For this purpose, the implemented functionality, which primarily provides the dispersibility, can be exploited as the chemical driving force to steer the formation of active device layers on pretreated surfaces. A well-developed approach to modify a surface is the use of self-assembled monolayers (SAMs), which typically consist of a simple n-alkyl chain of sp^3-carbon species, an anchor group and a functional headgroup, responsible for tuning the surface properties.[28,29] The headgroup can be tailored to fit to the functional moieties of the carbon allotropes to allow for strong interactions between the insulating SAM with the active carbon allotropes. Additional to the sp^2-based carbon allotropes with the insulating sp^3 alkyl chained SAMs, all components (conductor, semiconductor and insulator) are available to develop fully carbon-based electronics.[30]

In the present work, we report on concepts that allow for the selective self-assembly of 0D, 1D and 2D carbon allotropes (Figure 1) in the active channel area of thin-film transistor (TFT) devices. These carbon allotropes are introduced to the channel area by a dip-coating approach, in which the substrate is simply immersed into the carbon allotrope solution. The devoted chemical functionalization provides surface interactions, leading to a self-aligned deposition. Due to the specificity in chemical interaction, the self-assembly is a self-terminated process, resulting in a confined channel layer thickness of almost monolayers of the corresponding C_{60}, CNTs or graphene. All devices consist of tiny hybrid dielectrics with 3.6 nm aluminum oxide (AlO_x) and insulating SAMs of different chemical composition in order to provide the attractive surface for the self-assembly of the carbon species. The hybrid stack (AlO_x/SAM) enables low-voltage transistor operation of less than 3 V.[31−34]

Self-assembled monolayer field-effect transistors (SAMFETs) of C_{60} were realized by a direct exchange reaction of stearic acid (C_{17}−CA) by C_{60}-functionalized octadecylphosphonic acids ($C_{60}C_{18}$−PA, Figure 2a), based on the difference of covalent bonding energies of phosphonic acids (PAs) and carboxylic acids (CAs) to AlO_x. For self-assembled SWCNT devices, we exploited the electrostatic interaction between a gate dielectric SAM 1-methyl-3-(dodecylphosphonic acid)imidazolium bromide (IMI-C_{12}−PA), which has a cationic imidazolium headgroup, and SWCNTs, which were noncovalently functionalized with a perylene bisimide derivative (Figure 3a). Functional graphene-based transistors were fabricated by self-assembly of GO flakes on the IMI-C_{12}−PA SAM, driven by the strong electrostatic attraction between the headgroup of the SAM and the GO. The GO flakes in the channel region were reduced from GO to rGO (Figure 4a).

To ensure that the selective self-assembly of the carbon allotropes is only attributed to the surface chemistry rather than to the surface roughness of the transistor gate pattern ($R_{RMS} \approx 1.3$ nm),[34] the selectivity was first investigated on flat atomic layer deposition (ALD) AlO_x substrates ($R_{RMS} \approx 0.5$ nm). The AlO_x substrates serve an in-plane pattern of different SAMs with attractive and nonattractive interactions of the carbon allotropes (detailed description in the Supporting Information).

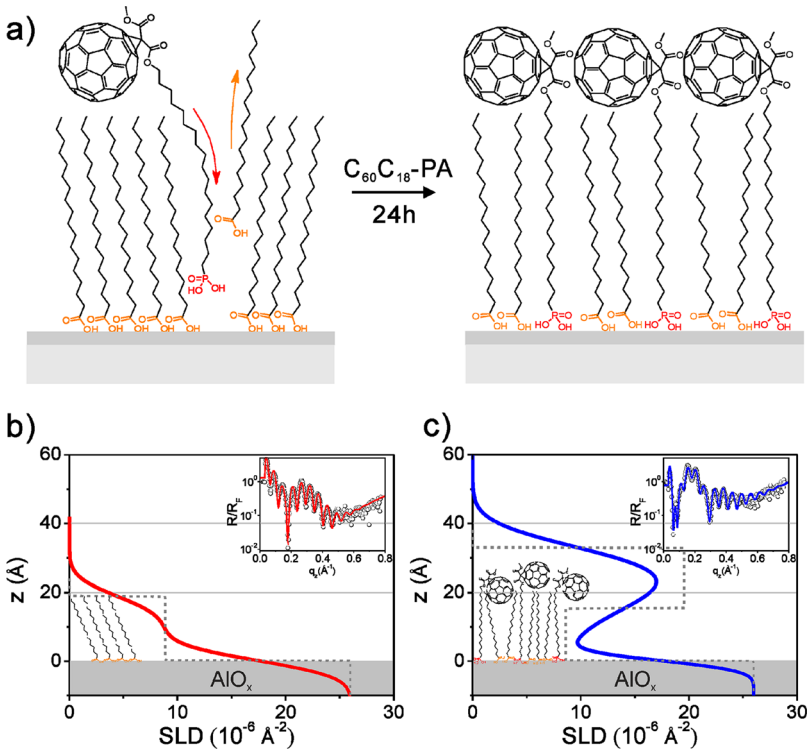

Figure 2. The region-selective deposition of $C_{60}C_{18}$—PA. (a) Schematic process of the exchange reaction, starting with a C_{17}—CA SAM, which is partially exchanged by $C_{60}C_{18}$—PA until saturation. (b and c) The best fit SLD profiles from X-ray reflectivity (XRR) measurements on a C_{17}—CA SAM before (b) and after (c) the exchange reaction with $C_{60}C_{18}$—PA. The measured reflectivity data are shown in the insets.

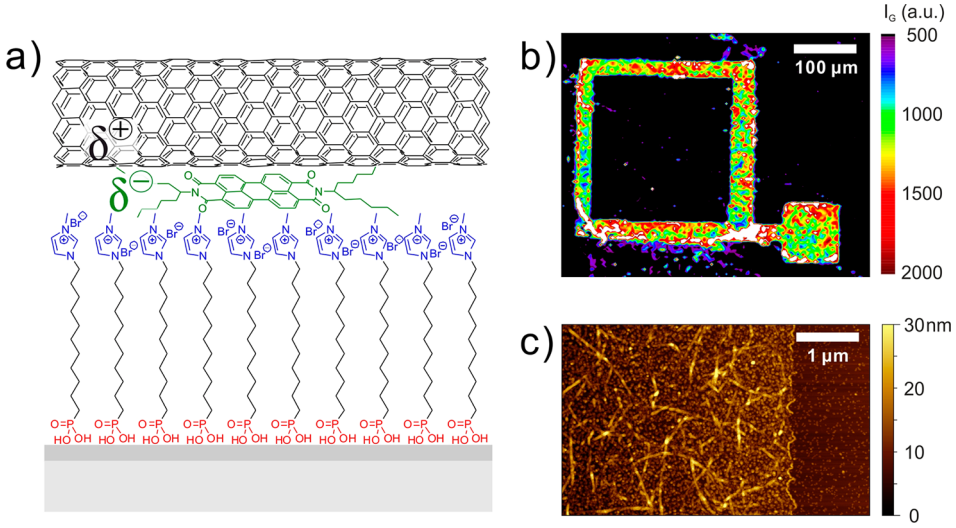

Figure 3. The region-selective deposition of the noncovalently functionalized SWCNTs. (a) Schematic sketch of proposed surface interaction of SWCNT on AlO_x surface functionalized with IMI-C_{12}—PA. The noncovalently functionalization (PBI in green color) interacts with SWCNT and leads to the formation of an electrostatic double layer indicated by δ^-/δ^+. Consequently, the PBI tends to attract the SWCNT to the positively charged SAM. (b) Raman spectroscopy mapping, considering G-band of the SWCNTs, illustrates the selective deposition of the SWCNTs onto the loop-structured region covered with IMI-C_{12}—PA. The other areas are functionalized with $F_{15}C_{18}$—PA SAM. (c) AFM image illustrating an edge region of the functionalized areas as in (b).

RESULTS AND DISCUSSION

Selective Self-Assembly of $C_{60}C_{18}$—PA. The use of solution processed C_{60}-terminated molecules as SAMs was demonstrated successfully as contact treatment layer in organic photovoltaic (OPV) devices,[35,36] as memory or photoreactive dielectric layer in organic TFTs[37,38] or even as active channel layer in SAMFETs.[33,39,40] For all examples, a direct deposition of the functionalized C_{60} derivatives on the bare oxide surface was used to create the SAMs. In particular for SAMFETs, the

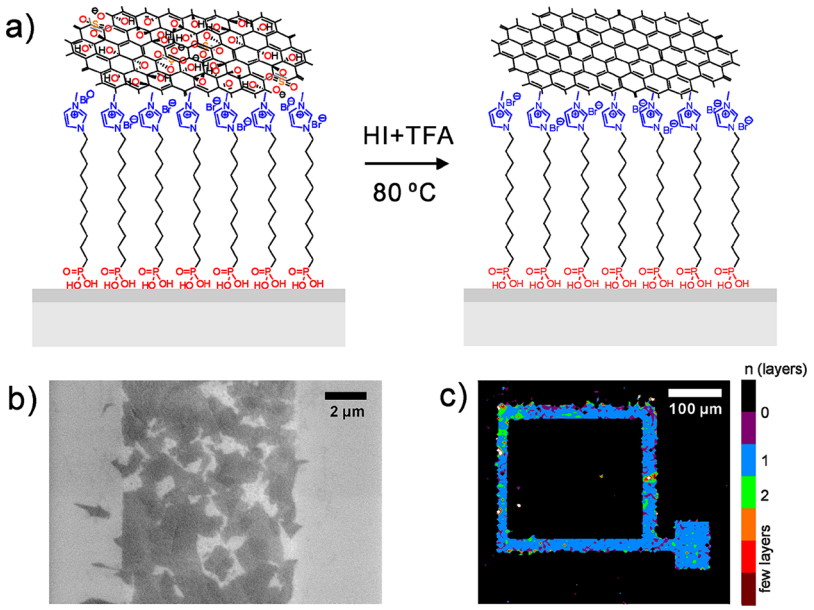

Figure 4. The region-selective deposition of GO. (a) The schematic interaction of GO on IMI-C_{12}—PA functionalized surface and the reduction process leading to a selective deposition of graphene flakes. The reduction agents are HI and TFA and the reaction temperature is 80 °C. (b) SEM image showing the selective deposition of GO. The regions with enrichment of GO flakes are functionalized by IMI-C_{12}—PA SAM and others are covered by $F_{15}C_{18}$—PA SAM layer. (c) Raman mapping showing the layer number of the rGO flakes, according to the intensity of the G-band. The measurement was taken from samples in (b) after the reduction process. The loop structure is covered by IMI-C_{12}—PA SAM, and the rest is covered by $F_{15}C_{18}$—PA SAM.

transport properties strongly depend on the effective $\pi-\pi$ interaction of the C_{60} head groups to form conductive pathways. Due to the mismatches between the required space of the C_{60} head groups and the PA anchor groups, the confined 2D order of C_{60} moieties is limited in such monolayers. It can be enhanced by mixing the fullerene functionalized molecules with alky-phosphonic acids to form a mixed monolayer of, *e.g.*, decylphosphonic acid (C_{10}-PA) and $C_{60}C_{18}$—PA, where the C_{10}-PA acts as a supporting feature.[40] Here, we present a new approach for a selective assembly of C_{60}-functionalized PAs, which simultaneously forces those active molecules to order, by partially exchanging SAMs of carboxylic acids. SAM molecules with CA anchor groups (binding energy on $AlO_x \approx -95$ kJ/mol) tend to be exchanged by stronger binding PAs (binding energy on $AlO_x \approx -178$ kJ/mol), with a driving force of −83 kJ/mol, but not *vice versa*.[41,42] That means in case of an in-plane patterned SAM surface consisting of a fluorinated SAM with PA anchor group (Figure 1a, green) and C_{17}—CA, only the CA is exchanged, leading to a selective deposition of $C_{60}C_{18}$—PA in this area.

Figure 2a shows the schematic of the exchange reaction performed over a period of 24 h by dip-coating the substrate into a 5.8 mg/L solution of $C_{60}C_{18}$—PA in 2-propanol. The scattering length density (SLD = $\rho_e \cdot r_e$, where ρ_e is the electron density, and r_e is the classical electron radius) profiles extracted from X-ray reflectivity (XRR) measurements[40] of the initial C_{17}—CA and the exchanged SAM are shown in Figures 2b,c (detailed description in the Supporting Information). The exchanged SAM consists of a mixture of both C_{17}—CA and $C_{60}C_{18}$—PA, where the shorter C_{17}—CA is partially exchanged by the PA connected to the C_{18} chain. We suppose that the exchange reaction proceeds until the $C_{60}C_{18}$—PA forms a densely packed C_{60} head layer. Underneath this C_{60} layer, the remaining C_{17}—CA prevents the C_{60} head groups from collapsing onto the substrate. The peak at 23 Å in the SLD profile (Figure 2c) indicates such a confined C_{60} arrangement. A clearly reduced SLD is detected between the AlO_x substrate and the C_{60} head groups corresponding to the alkyl chains of C_{17}—CA and $C_{60}C_{18}$—PA, compared to a pure $C_{60}C_{18}$—PA SAM (Figure S1). The remain of CAs after the exchange reaction was further proven by X-ray photoelectron spectroscopy (XPS) of 4,4,5,5,6,6,7,7,8,8,9,9,10,10,11,11,11-heptadecauoroundecanoic acid ($F_{17}C_{10}$-CA, utilized to obtain a clear XPS signal) exchanged by $C_{60}C_{18}$—PA (Figure S2).

Selective Self-Assembly of Functionalized SWCNTs. Specific surface treatment with SAMs has already been demonstrated to assemble SWCNTs in transistor channels.[8,43] In the present approach, the SWCNTs are noncovalently functionalized with *N,N′*-bis(1-pentylhexyl)perylene-3,4:9,10-tetracarboxylic bisimide (PBI) (Figure 3a) that is soluble in most organic solvents such as *N,N*-dimethylformamide (DMF). PBIs have demonstrated high dispersion and individualization rates of SWCNTs *via* $\pi-\pi$ stacking in aqueous solution, while leaving the carbon lattice intact.[44,45] We used a batch of pristine SWCNTs, consisting of a mixture of both metallic- and semiconducting-nanotubes, allowing for a high throughput of our device production and optimization of the process. Further work will concentrate on the improvement of

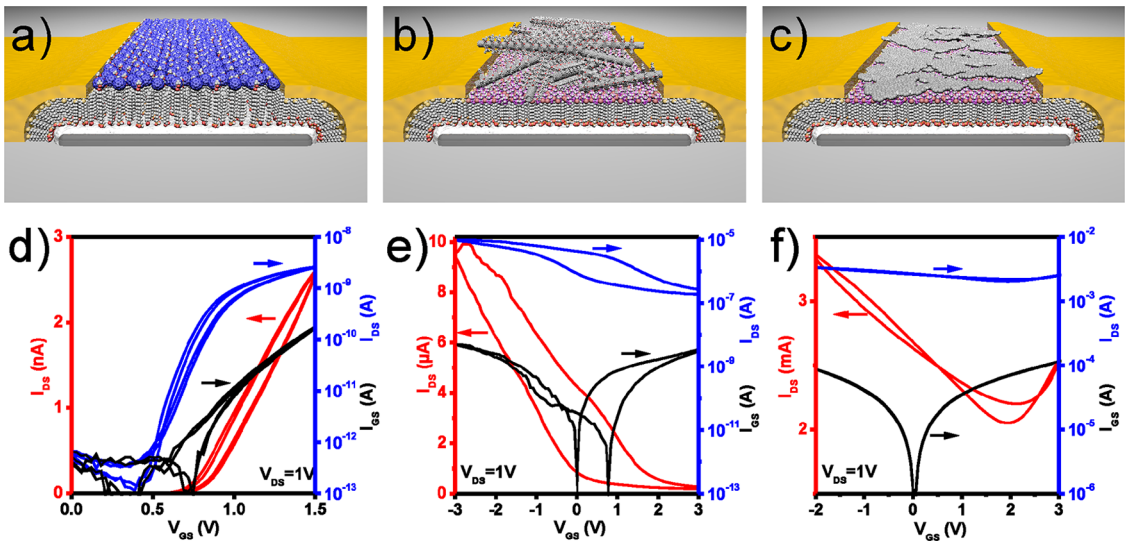

Figure 5. The schematic device architectures and electric characteristics of the devices based on region-selectively deposited carbon allotropes. FETs based on (a) $C_{60}C_{18}$—PA, (b) SWCNTs and (c) rGO. (d—f) Corresponding transfer curves of the devices from (a) to (c), respectively. The channel length *L* and channel width *W* for the C_{60}-based devices are $L = 3\ \mu m$ and $W = 100\ \mu m$ and for the SWCNT- and rGO-based devices are $L = 5\ \mu m$ and $W = 1000\ \mu m$.

mentioned devices by utilizing highly purified s-SWCNTs (detailed description in the Supporting Information).

The prepatterned substrates consist of SAMs on the ALD-AlO_x of 12,12,13,13,14,14,15,15,16,16,17,17,18,18,18-pentadecafluorooctadecyl-phosphonic acid ($F_{15}C_{18}$—PA) and IMI-C_{12}—PA, which provides a positively charged imidazolium headgroup. They were dip-coated into the SWCNT solution with a concentration of 0.06 mg/mL for 24 h. The PBI ligands act as p-dopants of the SWCNTs.[46] The interaction between PBIs and SWCNTs increases the electron density in the noncovalently attached PBI and leads to a negative ζ-potential of −22 mV. The PBI functionalized SWCNTs exhibit a negatively polarized layer and are hence easily attracted by the positively charged IMI-C_{12}—PA surface. This driving force is used to place SWCNTs on specific patterns of IMI-C_{12}—PA but not on $F_{15}C_{18}$—PA. Since PBI is a neutral molecule in its pure form, the remaining free PBI is likely not interacting with the IMI-C_{12}—PA surface. Consequently, the free PBI is not affecting the SWCNT deposition and makes a further purification or dialysis step unnecessary.[8]

The selective deposition of SWCNTs has been confirmed by scanning Raman spectroscopy mapping of the G-band intensity, as intrinsic feature of the sp^2-carbon species (Figure 3b), as well as atomic force microscope (AFM) measurements (Figure 3c). The region with pronounced G-band intensity is covered with the positively charged IMI-C_{12}—PA SAM, which is attractive for SWCNTs, while the black region is covered with $F_{15}C_{18}$—PA SAM. An AFM image from the edge of the patterned structure shows a digital placement of the SWCNTs. The solution-based SWCNTs are appearing as a random network on the substrate.

Since the selective self-assembly process is driven by the attractive Coulomb force, it is not limited to those SAM-couples with a large difference in surface energies like $F_{15}C_{18}$—PA (γ = 9 mN/m)[47] and IMI-C_{12}—PA (γ = 62 mN/m). The same tendency was found by using a thiol-terminated SAM 12-mercaptododecylphosphonic acid (HS-C_{12}—PA) with surface energy of 45 mN/m. A selective placement of SWCNTs onto IMI-C_{12}—PA in contrast to the HS-C_{12}—PA (Figure S3) was proven by AFM and Raman characterizations. The employing of HS-C_{12}—PA is further beneficial to utilize stronger adhesion of gold source/drain electrodes in fabrication of fully integrated transistor devices and to make the processing more reliable than using $F_{15}C_{18}$—PA (Figure 5b).

Selective Self-Assembly of GO and Conversion to rGO. The oxidation of graphite enables the solution-based self-assembly of graphene materials and even the functional groups attached to GO could provide a driving force for selective self-assembled deposition. In literature, the selective deposition of GO has been realized based on the difference in surface energy of the SAM surface.[48,49] However, the selective deposition should not be limited only to the difference in surface energy but also (as described in case of SWCNTs) could be driven by a stronger interaction such as the electrostatic force, resulting in a higher degree of selectivity. The routine for our process consists of the deposition of the GO on dedicated SAMs and the reduction process by converting GO to flakes of rGO, as shown in Figure 4a.

GO is produced by a recently published method, and the yielded GO bears an almost preserved σ-framework of carbon atoms and is chemically functionalized by hydroxyl, epoxy and organosulfate as major groups (detailed description in the Supporting Information).[50,51] Due to these negatively charged groups, the GO exhibits a negative ζ-potential of about −50 mV.[51] The same prepatterned IMI-C_{12}—PA and

$F_{15}C_{18}$—PA SAM layers (as used for self-assembly of SWCNTs) provide selective deposition sites with the imidazolium headgroup for GO flakes. The driving force for the selective deposition of GO is an electrostatic attraction of the negatively charged GO and the positively charged IMI-C_{12}—PA SAM headgroup.

The prepatterned ALD substrate is dip-coated into the GO dispersion (0.1 mg/mL) for 24 h. The resulting selective deposition of GO on the substrate is visualized with scanning electron microscope (SEM) shown in Figure 4b. As presented in the SEM image, most of the IMI-C_{12}—PA region is covered by the GO flakes. On the basis of the gray scale of the SEM image, the average coverage by GO on the surface is up to 86%, regardless of mono-, bi-, or few layer flakes.

The selective deposition of GO flakes on the substrate is followed by a reduction process in the atmosphere of hydriodic acid (HI) and trifluoroacetic acid (TFA) at 80 °C (detailed description in the Supporting Information).[50,52,53] To identify the number of deposited rGO layers, the G-band intensity is measured using scanning Raman microscopy (Figure 4c).[54] The typical Raman spectrum of the rGO and the mapping of G-band intensity, D-band intensity and the intensity ratio of the D- and G-bands are presented in Figure S4. From the Raman mapping image and the analysis of the G-band intensity histogram (Figure S5), we estimate coverage of the IMI-C_{12}—PA SAM region of about 78% with detectable G-band, in which there are about 74% monolayers, 14% bilayers and about 12% few layers. This high coverage is in good agreement with the results from SEM measurements, confirming the efficiency of the self-assembly process.

TFTs Based on Self-Assembled Carbon Allotropes. To validate the highly region-selective deposition of all aforementioned functionalized carbon allotropes, the process was applied in the fabrication of TFTs. The device preparation for all the materials are based on standard photolithography processes (detailed description in the Supporting Information). The schematic profiles of the devices for C_{60}-, SWCNTs- and GO-based materials are illustrated in Figures 5a—c, respectively. All devices are fabricated in bottom-gate bottom-contact configuration.

For $C_{60}C_{18}$—PA-based SAMFETs, an expected n-type TFT transport property[12] is achieved (as indicated in the transfer curve of Figure 5d) with a threshold voltage of V_{th} = 0.5 V. The on/off-current ratio reaches as high as 8×10^3, indicating a perfect switch ability. For the geometry with channel length of 3 μm and width of 100 μm, the obtained on- and off-currents are 2.6×10^{-9} and 3.3×10^{-13} A, respectively. The source/drain-gate overlap regions are covered with insulating C_{17}—CA. For the on-state region of the FET, the drain current is at least 1 order of magnitude larger than the gate leakage current. Besides, the charge carrier mobility in the saturation regime is 3.0×10^{-4} $cm^2 V^{-1} s^{-1}$. This value exceeds the mobility in devices with direct self-assembled pure $C_{60}C_{18}$—PA by 1 order of magnitude (Figures S6 and S7).

The TFTs based on the random network of functionalized SWCNTs on IMI-C_{12}—PA SAM were fabricated and measured in ambient air. The transistor characteristics of a Corbino geometry[55,56] with channel length of 5 μm and width of 1000 μm (Figure S8a, left) is presented in Figure 5e. The maximum on-/off-current ratio at the interval of V_{GS} = −3.0 to 3.0 V reaches to 50.6, and the I_{DS}/I_{GS} ratio at V_{GS} = −3.0 V is 1.87×10^3. By considering the random network of SWCNTs in the channel as a thin film, the conventional equation of the mobility in linear regime is valid for the present devices. This linear mobility leads to a value of 0.02 $cm^2 V^{-1} s^{-1}$. It is worth noting that the TFT characteristics such as mobility and/or on-/off-current ratio can be improved by applying our concept to higher concentrated solutions of CNTs and/or purely semiconducting-SWCNTs with advanced aspect ratio.[43,57] A doubled concentration of CNT solution (0.12 mg/mL), assembled under the same conditions and into the same device setup, leads to an improved linear mobility of 0.56 cm^2 V^{-1} s^{-1} (Figure S9).

For a device based on rGO, which has the same geometry and architecture as SWCNT-based TFTs, a typical transfer curve measured in ambient air is shown in Figure 5f. The devices exhibit a Dirac voltage of V_{GS} = 1.95 V with considerable symmetric electron- and hole-conductions, especially in the sense of the transconductance of the transistor. The current modulation ratio could reach to the value of 1.6, and the I_{DS}/I_{GS} ratio is at least 1 order of magnitude. The extracted linear mobility for electrons and holes is 3.20 and 1.75 $cm^2 V^{-1} s^{-1}$, respectively. These values driven by an internal field are much higher than those from a self-assembly driven by an external electrostatic force.[58] The corresponding output curves for all the TFTs are presented in Figure S8.

CONCLUSIONS

We have presented a general approach for region-selective self-assembly of 0D, 1D and 2D carbon allotropes from solution. By tuning the interaction between a modified surface and functionalized carbon allotropes, the carbon species can be directed to a dedicated target area. This general concept was proven to work for functionalized fullerenes, carbon nanotubes and graphene as our model systems. In case of the fullerenes, a covalent functionalization with an alkyl phosphonic acid was chosen, and a surface specific self-assembly of areas covered with SAMs of carboxylic acids was shown. For the SWCNTs, a noncovalent functionalization with PBI derivatives was adopted, which enabled stable dispersions in common organic solvents and introduced an attractive interaction to charged surfaces. Aluminum oxide, modified with charged self-assembled monolayers of IMI-C_{12}—PA, served as target

surface. As an example of a 2D system, GO was prepared from graphite and dispersed in an aqueous solution. The necessary oxidation process introduces covalently bound and charged moieties on the carbon system, which can be utilized to establish attractive forces to an oppositely charged surface. In the present work, this charged surface was realized by a SAM of IMI-C_{12}—PA. For all three systems, we managed to apply the assembly approach of carbon allotropes to the channel region of fully patterned TFTs, yielding operating transistor devices.

METHODS

Preparation of Photolithographically Patterned Substrates. For the preparation, heavily p-doped silicon wafers with an aluminum oxide layer of 10 nm thickness formed by atomic layer deposition (ALD) were used. The wafer was treated with oxygen plasma for 3 min (pressure 0.2 mbar, power 200 W) to enrich the hydroxyl groups on the surface. A monolayer was self-assembled on the flat surface by immersion into a 0.025 mmol/L solution of IMI-C_{12}—PA (2-propanol as solvent) for 4 h. A 30 nm layer of gold was evaporated as a sacrificial layer to protect the IMI-C_{12}—PA SAM from the photoresist material. After the photolithographical patterning and wet-chemical etching of the gold layer, IMI-C_{12}—PA was removed from the exposed regions by 10 min of oxygen plasma treatment. Afterward, fluorinated SAM was assembled on the bare aluminum oxide by immersion into 0.2 mmol/L solution of $F_{15}C_{18}$—PA (2-propanol as solvent) for 24 h. The process is illustrated in Figure S10.

The Raman Mapping Method for Visualization of the Selective Deposition. Raman spectroscopic studies were performed on Horiba Jobin Yvon LabRAM Aramis confocal Raman spectrometer equipped with a microscope and an automated XYZ table, at laser excitation of 532 nm. The increment for scanning Raman microscopy was 4 μm and the laser energy was 2 mW.

The selective deposition of SWCNTs was visualized by scanning Raman microscopy and intensity of the G-band was measured as shown in Figure 3b. The black area denotes the substrate without SWCNT coverage and the colored area implies the region of self-deposited SWCNTs.

To visualize the number of layer of rGO over the scanned area, the G-band intensity of Raman spectra was used to finally distinguish between uncovered substrate (black), monolayers of graphene (blue), bilayers of graphene (green) and few layers of graphene (red), as shown in Figure 4c.

Conflict of Interest: The authors declare no competing financial interest.

Supporting Information Available: Description of utilized materials, further measurements, device fabrication procedure and additional figures. This material is available free of charge *via* the Internet at http://pubs.acs.org.

Acknowledgment. We acknowledge gratefully the German Research Council (DFG), the Collaborative Research Center 953, the Cluster of Excellence "Engineering of Advanced Materials – EXC 315" (www.eam.uni-erlangen.de) and the Erlangen Graduate School of Molecular Science (GSMS) for financial support.

REFERENCES AND NOTES

1. Guldi, D. M.; Illescas, B. M.; Atienza, C. M.; Wielopolski, M.; Martin, N. Fullerene for Organic Electronics. *Chem. Soc. Rev.* **2009**, *38*, 1587–1597.
2. Avouris, P. Carbon-Based Electronics. *Nat. Nanotechnol.* **2007**, *2*, 605–615.
3. Geim, A.; Novoselov, K. The Rise of Graphene. *Nat. Mater.* **2007**, *6*, 183–191.
4. Burghard, M.; Klauk, H.; Kern, K. Carbon-Based Field-Effect Transistors for Nanoelectronics. *Adv. Mater.* **2009**, *21*, 2586–2600.
5. Schwierz, F. Graphene Transistors. *Nat. Nanotechnol.* **2010**, *5*, 487–496.
6. Wang, Z.; Zhang, Z.; Peng, L.-M. Graphene-Based Ambipolar Electronics for Radio Frequency Applications. *Chin. Sci. Bull.* **2012**, *57*, 2956–2970.
7. Bae, S.; Kim, H.; Lee, Y.; Xu, X.; Park, J.-S.; Zheng, Y.; Balakrishnan, J.; Lei, T.; Ri Kim, H.; Song, Y. I.; *et al.* Roll-to-Roll Production of 30-Inch Graphene Films for Transparent Electrodes. *Nat. Nanotechnol.* **2010**, *5*, 574–578.
8. Park, H.; Afzali, A.; Han, S.-J.; Tulevski, G. S.; Franklin, A. D.; Tersoff, J.; Hannon, J. B.; Haensch, W. High-Density Integration of Carbon Nanotubes *via* Chemical Self-Assembly. *Nat. Nanotechnol.* **2012**, *7*, 787–791.
9. Zhu, W.; Farmer, D. B.; Jenkins, K. A.; Ek, B.; Oida, S.; Li, X.; Bucchignano, J.; Dawes, S.; Duch, E. A.; Avouris, P. Graphene Radio Frequency Devices on Flexible Substrate. *Appl. Phys. Lett.* **2013**, *102*, 233102.
10. Xu, H.; Zhang, Z.; Shi, R.; Liu, H.; Wang, Z.; Wang, S.; Peng, L.-M. Batch-Fabricated High-Performance Graphene Hall Elements. *Sci. Rep.* **2013**, *3*, 1207.
11. Gaudiana, R.; Brabec, C. Organic Materials: Fantastic Plastic. *Nat. Photonics* **2008**, *2*, 287–289.
12. Anthony, J. E.; Facchetti, A.; Heeney, M.; Marder, S. R.; Zhan, X. n-Type Organic Semiconductors in Organic Electronics. *Adv. Mater.* **2010**, *22*, 3876–3892.
13. Wilder, J. W. G.; Venema, L. C.; Rinzler, A. G.; Smalley, R. E.; Dekker, C. Electronic Structure of Atomically Resolved Carbon Nanotubes. *Nature* **1998**, *391*, 59–62.
14. Saito, R.; Dresselhaus, G.; Dresselhaus, M. S. *Physical Properties Of Carbon Nanotubes*; Imperial College Press: London, 1998.
15. Weiss, N. O.; Zhou, H.; Liao, L.; Liu, Y.; Jiang, S.; Huang, Y.; Duan, X. Graphene: An Emerging Electronic Material. *Adv. Mater.* **2012**, *24*, 5782–5825.
16. Ding, L.; Zhang, Z.; Liang, S.; Pei, T.; Wang, S.; Li, Y.; Zhou, W.; Liu, J.; Peng, L.-M. CMOS-Based Carbon Nanotube Pass-Transistor Logic Integrated Circuits. *Nat. Commun.* **2012**, *3*, 677.
17. Liao, L.; Lin, Y.-C.; Bao, M.; Cheng, R.; Bai, J.; Liu, Y.; Qu, Y.; Wang, K. L.; Huang, Y.; Duan, X. High-Speed Graphene Transistors with a Self-Aligned Nanowire Gate. *Nature* **2010**, *467*, 305–308.
18. Wu, Y.; Farmer, D. B.; Xia, F.; Avouris, P. Graphene Electronics: Materials, Devices, and Circuits. *Proc. IEEE* **2013**, *101*, 1620–1637.
19. Hummelen, J. C.; Knight, B. W.; LePeq, F.; Wudl, F.; Yao, J.; Wilkins, C. L. Preparation and Characterization of Fulleroid and Methanofullerene Derivatives. *J. Org. Chem.* **1995**, *60*, 532–538.
20. Chikamatsu, M.; Nagamatsu, S.; Yoshida, Y.; Saito, K.; Yase, K.; Kikuchi, K. Solution-Processed n-Type Organic Thin-Film Transistors with High Field-Effect Mobility. *Appl. Phys. Lett.* **2005**, *87*, 203504.
21. Nish, A.; Hwang, J.-Y.; Doig, J.; Nicholas, R. J. Highly Selective Dispersion of Single-Walled Carbon Nanotubes Using Aromatic Polymers. *Nat. Nanotechnol.* **2007**, *2*, 640–646.
22. Vaisman, L.; Wagner, H. D.; Marom, G. The Role of Surfactants in Dispersion of Carbon Nanotubes. *Adv. Colloid Interface Sci.* **2006**, *128–130*, 37–46.
23. Hersam, M. C. Progress towards Monodisperse Single-Walled Carbon Nanotubes. *Nat. Nanotechnol.* **2008**, *3*, 387–394.
24. Usrey, M. L.; Strano, M. S. Controlling Single-Walled Carbon Nanotube Surface Adsorption with Covalent and Noncovalent Functionalization. *J. Phys. Chem. C* **2009**, *113*, 12443–12453.
25. Dreyer, D. R.; Park, S.; Bielawski, C. W.; Ruoff, R. S. The Chemistry of Graphene Oxide. *Chem. Soc. Rev.* **2010**, *39*, 228–240.
26. Mao, S.; Pu, H.; Chen, J. Graphene Oxide and Its Reduction: Modeling and Experimental Progress. *RSC Adv.* **2012**, *2*, 2643–2662.

27. Eigler, S.; Enzelberger-Heim, M.; Grimm, S.; Hofmann, P.; Kroener, W.; Geworski, A.; Dotzer, C.; Röckert, M.; Xiao, J.; Papp, C.; *et al.* Wet Chemical Synthesis of Graphene. *Adv. Mater.* **2013**, *25*, 3583–3587.
28. Yan, Z.; Sun, Z.; Lu, W.; Yao, J.; Zhu, Y.; Tour, J. M. Controlled Modulation of Electronic Properties of Graphene by Self-Assembled Monolayers on SiO_2 Substrates. *ACS Nano* **2011**, *5*, 1535–1540.
29. Salinas, M.; Jäger, C. M.; Amin, A. Y.; Dral, P. O.; Meyer-Friedrichsen, T.; Hirsch, A.; Clark, T.; Halik, M. The Relationship between Threshold Voltage and Dipolar Character of Self-Assembled Monolayers in Organic Thin-Film Transistors. *J. Am. Chem. Soc.* **2012**, *134*, 12648–12652.
30. Li, B.; Cao, X.; Ong, H. G.; Cheah, J. W.; Zhou, X.; Yin, Z.; Li, H.; Wang, J.; Boey, F.; Huang, W.; *et al.* All-Carbon Electronic Devices Fabricated by Directly Grown Single-Walled Carbon Nanotubes on Reduced Graphene Oxide Electrodes. *Adv. Mater.* **2010**, *22*, 3058–3061.
31. Halik, M.; Klauk, H.; Zschieschang, U.; Schmid, G.; Dehm, C.; Schutz, M.; Maisch, S.; Effenberger, F.; Brunnbauer, M.; Stellacci, F. Low-Voltage Organic Transistors with an Amorphous Molecular Gate Dielectric. *Nature* **2004**, *431*, 963–966.
32. Klauk, H.; Zschieschang, U.; Pflaum, J.; Halik, M. Ultralow-Power Organic Complementary Circuits. *Nature* **2007**, *445*, 745–748.
33. Novak, M.; Ebel, A.; Meyer-Friedrichsen, T.; Jedaa, A.; Vieweg, B. F.; Yang, G.; Voitchovsky, K.; Stellacci, F.; Spiecker, E.; Hirsch, A.; *et al.* Low-Voltage p- and n-Type Organic Self-Assembled Monolayer Field Effect Transistors. *Nano Lett.* **2011**, *11*, 156–159.
34. Schmaltz, T.; Amin, A. Y.; Khassanov, A.; Meyer-Friedrichsen, T.; Steinrück, H.-G.; Magerl, A.; Segura, J. J.; Voitchovsky, K.; Stellacci, F.; Halik, M. Low-Voltage Self-Assembled Monolayer Field-Effect Transistors on Flexible Substrates. *Adv. Mater.* **2013**, *25*, 4511–4514.
35. Ma, H.; Yip, H.-L.; Huang, F.; Jen, A. K.-Y. Interface Engineering for Organic Electronics. *Adv. Funct. Mater.* **2010**, *20*, 1371–1388.
36. Stubhan, T.; Salinas, M.; Ebel, A.; Krebs, F. C.; Hirsch, A.; Halik, M.; Brabec, C. J. Increasing the Fill Factor of Inverted P3HT:PCBM Solar Cells through Surface Modification of Al-Doped ZnO *via* Phosphonic Acid-Anchored C_{60} SAMs. *Adv. Energy Mater.* **2012**, *2*, 532–535.
37. Burkhardt, M.; Jedaa, A.; Novak, M.; Ebel, A.; Voïtchovsky, K.; Stellacci, F.; Hirsch, A.; Halik, M. Concept of a Molecular Charge Storage Dielectric Layer for Organic Thin-Film Memory Transistors. *Adv. Mater.* **2010**, *22*, 2525–2528.
38. Salinas, M.; Halik, M. Photoactive Self-Assembled Monolayers for Optically Switchable Organic Thin-Film Transistors. *Appl. Phys. Lett.* **2013**, *102*, 203301.
39. Rumpel, A.; Novak, M.; Walter, J.; Braunschweig, B.; Halik, M.; Peukert, W. Tuning the Molecular Order of C_{60} Functionalized Phosphonic Acid Monolayers. *Langmuir* **2011**, *27*, 15016–15023.
40. Jäger, C. M.; Schmaltz, T.; Novak, M.; Khassanov, A.; Vorobiev, A.; Hennemann, M.; Krause, A.; Dietrich, H.; Zahn, D.; Hirsch, A.; *et al.* Improving the Charge Transport in Self-Assembled Monolayer Field-Effect Transistors: From Theory to Devices. *J. Am. Chem. Soc.* **2013**, *135*, 4893–4900.
41. Lenz, T.; Schmaltz, T.; Novak, M.; Halik, M. Self-Assembled Monolayer Exchange Reactions as a Tool for Channel Interface Engineering in Low-Voltage Organic Thin-Film Transistors. *Langmuir* **2012**, *28*, 13900–13904.
42. Bauer, T.; Schmaltz, T.; Lenz, T.; Halik, M.; Meyer, B.; Clark, T. Phosphonate- and Carboxylate-Based Self-Assembled Monolayers for Organic Devices: A Theoretical Study of Surface Binding on Aluminum Oxide with Experimental Support. *ACS Appl. Mater. Interfaces* **2013**, *5*, 6073–6080.
43. LeMieux, M. C.; Roberts, M.; Barman, S.; Jin, Y. W.; Kim, J. M.; Bao, Z. Self-Sorted, Aligned Nanotube Networks for Thin-Film Transistors. *Science* **2008**, *321*, 101–104.
44. Backes, C.; Schmidt, C. D.; Hauke, F.; Böttcher, C.; Hirsch, A. High Population of Individualized SWCNTs through the Adsorption of Water-Soluble Perylenes. *J. Am. Chem. Soc.* **2009**, *131*, 2172–2184.
45. Backes, C.; Mundloch, U.; Schmidt, C. D.; Coleman, J. N.; Wohlleben, W.; Hauke, F.; Hirsch, A. Enhanced Adsorption Affinity of Anionic Perylene-Based Surfactants towards Smaller-Diameter SWCNTs. *Chem.—Eur. J.* **2010**, *16*, 13185–13192.
46. Ehli, C.; Oelsner, C.; Guldi, D. M.; Mateo-Alonso, A.; Prato, M.; Schmidt, C.; Backes, C.; Hauke, F.; Hirsch, A. Manipulating Single-Wall Carbon Nanotubes by Chemical Doping and Charge Transfer with Perylene Dyes. *Nat. Chem.* **2009**, *1*, 243–249.
47. Novak, M.; Schmaltz, T.; Faber, H.; Halik, M. Influence of Self-Assembled Monolayer Dielectrics on the Morphology and Performance of α,ω-Dihexylquaterthiophene in Thin Film Transistors. *Appl. Phys. Lett.* **2011**, *98*, 093302.
48. Cho, H. Y.; Han, C. J.; In, I. Site-Selective Deposition of Graphene Oxide Layer on Patterned Self-Assembled Monolayer. *Chem. Lett.* **2012**, *41*, 290–291.
49. Wu, C.; Cheng, Q.; Sun, S.; Han, B. Templated Patterning of Graphene Oxide Using Self-Assembled Monolayers. *Carbon* **2012**, *50*, 1083–1089.
50. Eigler, S.; Enzelberger-Heim, M.; Grimm, S.; Hofmann, P.; Kroener, W.; Geworski, A.; Dotzer, C.; Röckert, M.; Xiao, J.; Papp, C.; *et al.* Wet Chemical Synthesis of Graphene. *Adv. Mater.* **2013**, *25*, 3583–3587.
51. Eigler, S.; Dotzer, C.; Hof, F.; Bauer, W.; Hirsch, A. Sulfur Species in Graphene Oxide. *Chem.—Eur. J.* **2013**, *19*, 9490–9496.
52. Cui, P.; Lee, J.; Hwang, E.; Lee, H. One-Pot Reduction of Graphene Oxide at Subzero Temperatures. *Chem. Commun.* **2011**, *47*, 12370–12372.
53. Eigler, S.; Grimm, S.; Enzelberger-Heim, M.; Muller, P.; Hirsch, A. Graphene Oxide: Efficiency of Reducing Agents. *Chem. Commun.* **2013**, *49*, 7391–7393.
54. Englert, J. M.; Vecera, P.; Knirsch, K. C.; Schäfer, R. A.; Hauke, F.; Hirsch, A. Scanning-Raman-Microscopy for the Statistical Analysis of Covalently Functionalized Graphene. *ACS Nano* **2013**, *7*, 5472–5482.
55. Yang, C. L.; Zudov, M. A.; Knuuttila, T. A.; Du, R. R.; Pfeiffer, L. N.; West, K. W. Observation of Microwave-Induced Zero-Conductance State in Corbino Rings of a Two-Dimensional Electron System. *Phys. Rev. Lett.* **2003**, *91*, 096803.
56. Yan, J.; Fuhrer, M. S. Charge Transport in Dual Gated Bilayer Graphene with Corbino Geometry. *Nano Lett.* **2010**, *10*, 4521–4525.
57. Roberts, M. E.; LeMieux, M. C.; Sokolov, A. N.; Bao, Z. Self-Sorted Nanotube Networks on Polymer Dielectrics for Low-Voltage Thin-Film Transistors. *Nano Lett.* **2009**, *9*, 2526–2531.
58. Kobayashi, T.; Kimura, N.; Chi, J.; Hirata, S.; Hobara, D. Channel-Length-Dependent Field-Effect Mobility and Carrier Concentration of Reduced Graphene Oxide Thin-Film Transistors. *Small* **2010**, *6*, 1210–1215.